Learning Complexity to Guide Light-Induced Self-Organized Nanopatterns

Eduardo Brandao,[1] Anthony Nakhoul,[1] Stefan Duffner,[2] R. Emonet,[1] Florence Garrelie,[1] Amaury Habrard,[1,3] François Jacquenet,[1] Florent Pigeon,[1] Marc Sebban,[1] and Jean-Philippe Colombier[1,*]

[1]*Université Jean Monnet Saint-Etienne, CNRS, IOGS, Laboratoire Hubert Curien UMR 5516, F-42023, SAINT-ETIENNE, France*
[2]*Université de Lyon, INSA Lyon, CNRS, UCBL, LIRIS, UMR5205, F-69621 Villeurbanne, France*
[3]*Institut Universitaire de France (IUF), Paris, France*

(Received 21 June 2022; revised 20 December 2022; accepted 24 April 2023; published 30 May 2023)

Ultrafast laser irradiation can induce spontaneous self-organization of surfaces into dissipative structures with nanoscale reliefs. These surface patterns emerge from symmetry-breaking dynamical processes that occur in Rayleigh-Bénard-like instabilities. In this study, we demonstrate that the coexistence and competition between surface patterns of different symmetries in two dimensions can be numerically unraveled using the stochastic generalized Swift-Hohenberg model. We originally propose a deep convolutional network to identify and learn the dominant modes that stabilize for a given bifurcation and quadratic model coefficients. The model is scale-invariant and has been calibrated on microscopy measurements using a physics-guided machine learning strategy. Our approach enables the identification of experimental irradiation conditions for a desired self-organization pattern. It can be generally applied to predict structure formation in situations where the underlying physics can be approximately described by a self-organization process and data is sparse and nontime series. Our Letter paves the way for supervised local manipulation of matter using timely controlled optical fields in laser manufacturing.

DOI: 10.1103/PhysRevLett.130.226201

The emergence of instabilities and symmetry breaking leading to the formation of coherent structures, is one of the most fascinating aspects of the complex dynamics governing light-surface interaction [1–3]. When a randomly rough surface is subjected to ultrafast laser pulses, it enters a far-from-equilibrium state due to the repeated absorption of pulsed optical fields. As a result, the surface exhibits spontaneous spatial organization, which is oriented by energy gradients generated by laser polarization, giving rise to laser-induced periodic surface structures (LIPSS) [4]. These structures form under far-from-equilibrium conditions and can be triggered by capillary waves, convection rolls, and thermoconvective instabilities, [5–8] which persist through dissipative structures [9]. Eliminating the prevailing laser polarization effects reveals puzzling patterns emerging from a sequence of instabilities, inducing different types of complex patterns, ranging from chaos to six-fold symmetries [10]. The photoexcited matter undergoes a transition from a disordered state to a more coherent one, referred to as a strange attractor in the phase space of nonlinear dynamics. This transition results in a metastable state, defining a self-organization structuring regime. Through this self-organization process, the material surface can be sculpted seamlessly, enabling nanoscale manufacturing [11]. Understanding the selection mechanisms involved in this morphogenesis to gain control over the uniformity, symmetry, and size of the resulting surface patterns is a major research theme in laser processing for photonics metasurfaces, biomimetics, or catalysis functionalization. [12,13]. To apply statistical inference approaches to complex systems and achieve generalizability, advanced physics-guided machine learning strategies are essential. Upon laser irradiation, a hazy boundary separates self-organized and organized surface patterns. When a material is exposed to sufficiently intense laser irradiation, it tends to organize along the stationary electromagnetic fields due to scattered or excited waves [4,14] and self-organize in response to the random fluctuations of light absorption with a symmetry breaking with respect to polarization [15,16]. Light-oriented and self-assembled dynamical processes are inherently superimposed, and surface topographies evolve spatiotemporally toward equilibrium patterns that result from a complex competition between free energy dissipation imposing entropy production and spontaneous ordering. Consequently, any preexisting or transient organization can be disrupted by random perturbations, which can be amplified by positive feedback to lead the system toward new patterns. Ultrafast laser texturing has recently been used to obtain deep subwavelength periodic patterns, which raises questions about the relevant electromagnetic processes that drive the formation of these patterns well below the diffraction limit [17,18]. Various types of 2D surface patterning have been reported, including patterns with oriented, triangular, hexagonal, labyrinthine, or chaotic symmetries [19–22], featuring both positive and negative reliefs such as humps, bumps, peaks, and spikes [10]. To explain the remarkably uniform establishment of these patterns on the microscale

independently from the oriented near-field optical effects on the random local nanotopography, a more global and collective perspective is required [10,21]. Nanoscale fluid flows were shown to be driven by a complex interplay between electromagnetic, internal, and surface pressure forces which can become trapped due to the resolidification process [8,21] The deterministic approach to predict the underlying optical coupling processes is limited because it requires the artificial integration of fluctuating conditions induced by surface roughness. Transiently formed structures can become unstable under nonlinear amplification and bifurcate into more complex patterns that are not accurately described by classical approaches like Navier-Stokes combined with Maxwell equations. Nonetheless, the complex pattern landscape has been experimentally explored and can now be compared with mathematical models dedicated to nonlinear system dynamics.

The Kuramoto-Sivashinsky approach has become a paradigm for describing pattern formation and spatiotemporal chaos on surfaces eroded by ion bombardment, which ultimately reproduces ripple formation and other organized patterns [23]. A similar approach was initially proposed for laser-induced nanopatterns, although a clear physical picture has yet to be established [24]. Along similar lines, the Swift-Hohenberg (SH) dynamics has been identified as a relevant candidate for representing the observed complexity of convective instabilities with spatiotemporal features, such as chaos, rolls, and hexagons [25,26]. The SH approach has proven to be useful in identifying generic spatiotemporal dynamics of patterns in convective fluids [27,28], as well as curvature- and stress-induced pattern-formation transition [29]. The SH approach was formally deduced from the Navier-Stokes equations in the Boussinesq approximation, with thermal fluctuation effects in a fluid near the Rayleigh-Bénard instability [30].

The purpose of this Letter is to demonstrate that laser-induced pattern formation at the nanoscale can be efficiently characterized and predicted by a stochastic SH model that is variational in time and conservative in space. Our original strategy relies on the use of machine learning (ML) integrating partial physical information in the form of the SH model, which allows us to identify dominating stable modes for a set of parameters independently of initial roughness conditions. Incorporating data and prior knowledge is naturally expressed in terms of Bayesian inference, for which well-established domain-specific methods exist dating back to Laplace [31], but which cannot be applied in our experimental situation of few data and partial physical knowledge: in geophysics and climate science, where the physical process is well understood, methods focus on state reconstruction, known as data assimilation [32]; in physics, since states can be prepared, model calibration was developed [33], with recent advancements using ML [34] to integrate the parameters of either the full model or a correction to incomplete physical knowledge from

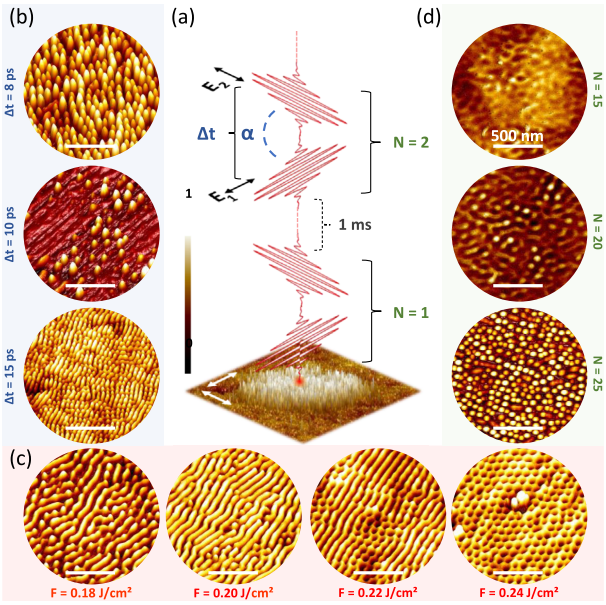

FIG. 1. (a) Schematic illustration of experimental self-organization regimes induced by bursts of ultrafast laser (150 fs) double pulses. (b) Self-organized patterns of topography that develop varying time delays for a given F and N (AFM-3D mode). (c) Nanopattern variation with respect to laser fluence at fixed Δt and N (AFM-3D mode). (d) Nanostructure growth by feedback at different number of pulses (AFM-2D mode), for a fixed Δt and F. The scale bars represent a length of 500 nm.

data [35]. However, solving the joint inverse problem of finding both state and model parameters is more challenging. In the climate sciences, sophisticated machine-learning techniques were recently proposed, integrating physical information via constraints, either during training or in model architecture itself [36–40], but require abundant time-series data. Our original strategy allows us to solve the dual inverse problem using only one observed state—a scanning electron microscope (SEM) image—even with little data. Furthermore, our modeling is scale invariant and can be applied to any laser process. By reducing experimental irradiation parameters to simple model coefficients, they can be optimized and extrapolated for surface pattern engineering.

Tailoring nanotopographic features on a surface is a challenging task that has been successfully accomplished using ultrafast laser processes with time-controlled polarization strategies. Numerous regimes of LIPSS have been reported with various periodicities, heights, orientations, and symmetries depending on different polarization directions between the first $\vec{E}_1$ and second pulse $\vec{E}_2$, characterized by $\sin\alpha = (\vec{E}_1\,\vec{E}_2)/(\|\vec{E}_1\|\,\|\vec{E}_2\|)$ in Fig. 1(a) [10,21,41,42]. Figs. 1(b)–1(d) present surface topographies measured by high resolution atomic force microscopy (AFM). A circular region with a diameter of 1 μm corresponding to the laser impact center was mapped in 3D (tilted) mode in Figs. 1(b) and 1(c) and in 2D for

Fig. 1(d). To observe the significant role of temporal pulse splitting Δt in nanopatterns control, laser peak fluence F and N were kept fixed at 0.18 J/cm^2 and 25, respectively, as shown in Fig. 1(b). At $\Delta t = 8$ ps, organized nanopeak structures were observed with a high aspect ratio, a height of ~100 nm and a diameter of ~20 nm [11]. An extension of 2 ps in Δt modifies the observed patterns that turn into a different organization, a regime referred to as nanobumps [10]. For $\Delta t = 15$ ps, a regime of nanohump generation is reached with a lower aspect ratio as the structures display a height of ≈10 nm and a diameter of ≈30 nm.

The role of laser fluence is revealed by fixing $\Delta t = 25$ ps and $N = 25$, as depicted in Fig. 1(c). At $F = 0.18$ J/cm^2, a low-contrast nanopeak regime is formed, evolving into a nanostripe pattern with a slight increase in laser fluence increase to 0.20 J/cm^2. At $F = 0.22$ J/cm^2, a transition region is established, combining both stripes and cavities. Finally, at $F = 0.24$ J/cm^2, the surface is uniformly organized with hexagonally arranged nanocavities having a depth of ≈25 nm and a diameter of ≈30 nm. Both nanohumps and nanovoids result from hydrothermal flows guided by surface tension and rarefaction forces, leading to thermoconvective instability at the nanoscale, similar to well-known Rayleigh-Bénard-Marangoni instabilities [8,10,21,43–54]. Laser dose also plays a role, as positive feedback regulates pulse-to-pulse topographical transformations. As shown in Fig. 1(d), at a fixed $F = 0.24$ J/cm^2 and $\Delta t = 8$ ps with different N, corresponding to the parameters of nanopeaks formation presented in Fig. 1(a), three different surface organizations were observed. Pulse-to-pulse growth dynamics exhibits the transitions from convection cells ($N = 15$), to the creation of crests on the convection cells ($N = 20$). The nanopeaks grow on the edges of the crests to reach their optimal shape, concentration, and organization at $N = 20$.

The adimensional form of the generalized SH equation used in this Letter is (see derivation in the Supplemental Material [55])

$$\dot{\tilde{u}} = \epsilon\tilde{u} - (1 + \tilde{\nabla}^2)^2\tilde{u} + \gamma\tilde{u}^2 - \tilde{u}^3. \tag{1}$$

The SH model was introduced in [30] as a model of Rayleigh-Bénard convection, modified by the inclusion of a u^2 nonlinearity allowing for small amplitude destabilization and the emergence of experimentally observed hexagonal patterns. With appropriate boundary conditions, the original SH equation exhibits a type-I-s instability that is isotropic, invariant with respect to translations and to $u \to -u$ [26]. Perturbations of $u_b = 0$ are selectively amplified depending on the norm of the wave number, leading to the formation of complex patterns with no preferential direction. The generalized SH model has the Lyapunov functional $\mathcal{L}[\tilde{u}] = \int_\Omega (\tilde{u}/2)(\nabla^4\tilde{u} + 2\nabla^2\tilde{u} + \tilde{u}) + \frac{1}{4}\tilde{u}^4 - (\gamma/3)\tilde{u}^3 - (\epsilon/2)\tilde{u}^2 d\mathbf{x}$ and $\dot{\tilde{u}} = -(\delta\mathcal{L}/\delta\tilde{u})$, as can be readily verified. During the SH dynamics, the Lyapunov functional $\mathcal{L}$ decreases in the same way as entropy decreases during the formation of physical patterns, and it converges asymptotically to a stable value [26] (see Fig. 2). We numerically solve the SH equation using a second-order Strang splitting pseudospectral solver with an adaptive time step [56–60], offering a good compromise between accuracy and speed. Figs. 2(a)–2(c) and Figs. 2(d)–2(f) show evolution dynamics of pattern formation for two pairs of ϵ, γ.

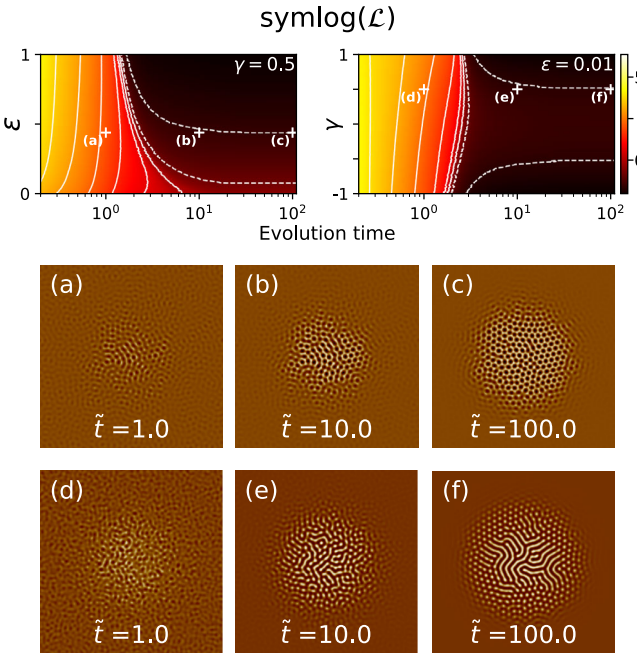

FIG. 2. Lyapunov functional of the generated field solutions of the SH equation as a function of evolution time $\tilde{t}$ for fixed ϵ and γ (ϵ a centered 2D Gaussian ramp to mimic the laser fluence distribution), depicted as a heat map in symlog scale, for independent initial conditions. Lyapunov functional evolution is largely independent of initial conditions and decreases during dynamics. The SH equation is able to reproduce, among others, highly symmetric hexagonal solutions (top), as well as labyrinthine solutions surrounded by nanopeaks.

A ML model is employed to learn the relationship between observed laser parameters θ and patterns, using only few, nontime series data (I), assuming an approximately SH process, not explicitly given in terms of θ, parametrized by ϕ (consisting of a scale factor l, the maximum wave number in a domain of side 224 pixels given as a multiple of 2π, the adimensional model parameters ϵ and γ, and $\tilde{t}$, which can be seen as a stabilization time) (II), with unknown initial conditions u_0 (III). We motivate this choice by symmetry considerations (Supplemental Material [55]) as well as the similarity between SEM images and SH solutions (Fig. 3). Combining experimental information with that obtained via the ML model, we find that the timescale of the convective instability is consistent with that reported in [10] (Supplemental Material [55]), further supporting our choice. Learning the relationship between laser parameters and

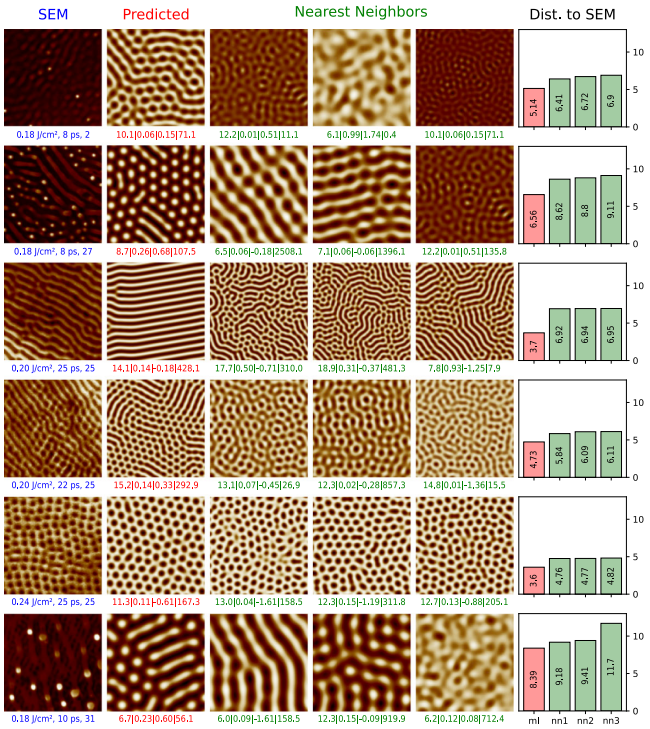

FIG. 3. Each row shows a 224 by 224 pixel SEM experimental image, with 1 μm ≈ 237 pixels which was never seen by the ML model during learning, the corresponding ML-predicted image for the same laser parameters, and three nearest neighbors (NN) of the former among solver generated images; and a bar plot of l_2 distance in the image of the feature mapping F_m between SEM image, ML-predicted image (ml), and NN (nn1, nn2, nn3). Image labels, left to right: F, Δt, N (SEM); predicted SH parameters l_p, ϵ_p, γ_p, $\tilde{t}_p$ (other). Bar plots: ML predictions are more accurate, as distance between SEM and ML predictions is smaller than to NN, the former integrating global information. On the first and second rows, NN with different length scales can be observed, suggesting concurrent multiscale SH processes. The ML model, which integrates single-scale SH knowledge, can only predict one of these processes.

patterns consists in solving the dual inverse problem of estimating an unknown initial state and model parameters with severe constraints, which is a challenging task and cannot be tackled, in general, using only ML methods. However, for a self-organization process, stating initial conditions exhaustively is wasteful, since for random perturbations of the uniformly zero solution of SH most Fourier modes are attenuated. Therefore, a feature mapping F_m is defined that is simplifying (noninjective) and discriminating [if u^i, u^j have different patterns then $F_m(u^i) \neq F_m(u^j)$] such that the image of the data distribution under F_m is conditionally independent of u_0 given the physical knowledge ϕ. This considerably simplifies the problem since the initial state no longer needs to be estimated. Learning F_m [61] from few data is impractical [62], (II) precludes deriving it on first principles, and, using traditional image features, would limit discriminating power for unknown patterns. F_m is, therefore, chosen as a deep convolutional neural network (CNN) [63] pretrained for a broad classification task on Imagenet [64], since CNNs are translation equivariant (making them suited for a pattern specification task). Their features are learned automatically from data, and retain scale information [65]. Given experimental data $\{\theta^i, u^i\}_{i=1,\ldots,N}$, we learn $\tilde{\phi}_\alpha$ that maximizes the log likelihood of the observed $F_m(u^i)$

$$\overline{\alpha} = \arg\max_{\alpha} \sum_{i=1}^{N} \log p[F_m(u^i)|\tilde{\phi}_\alpha(\theta^i)]. \tag{2}$$

Assuming that the distribution of ϕ given θ is peaky, we label experimental u^i with $\tilde{\phi}^i$ the SH parameters of its nearest neighbor (NN), in the image of F_m, among a large number of u pregenerated with the SH solver from random u_0. By integrating physical knowledge in this way, the problem of maximizing the likelihood above can be replaced with a lower bound. Explicitly, assuming data are sampled from independent and identically distributed Gaussian random variables,

$$\bar{\alpha} = \arg\min_{\alpha} \frac{1}{N} \sum_{i=1}^{N} \|\tilde{\phi}^i - \tilde{\phi}_\alpha(\theta^i)\|^2, \tag{3}$$

which is a low-dimensional problem that can be solved with few data [66] with a support vector regressor [67] $\tilde{\phi}_\alpha$ parametrized by α.

Figure 3 demonstrates the remarkable accuracy of our ML strategy in predicting the shape and scale of experimental patterns, even for never-before-seen laser parameters. Our strategy is more efficient than local methods that rely on nearest neighbor information, since the distance to the SEM experimental patterns in the image of the feature mapping F_m is smaller. As shown in Fig. 4, the complexity of the learned relationship between laser parameters and SH parameters grows with the number of experimental observations, with sharp boundaries of rapidly varying parameter values in regions of many data. The ML model can extrapolate to regions with few data for N and Δt, but less so for F, which would require higher experimental resolution. Importantly, we find that predicted SH parameters are correlated, and the correlation sign changes with N (Supplemental Material [55]): l_p, for example, is inversely correlated with pattern characteristic size and increases with N (the increase is not uniform, being greater for large l_p regions). This parameter is particularly important as the characteristic size of a stable mode is of great interest for applications. Because l_p and other parameters are correlated, it cannot be set freely; but as seen in Fig. 4, parameter isosurfaces are orthogonal at places: at, e.g., $N = 25$, a high-gradient transition regime for l_p, at $F = 0.18$ J/cm^2, $\Delta t = 15$ ps in the Δt direction is observed, while for F, Δt in the same region, the other SH parameters remain roughly

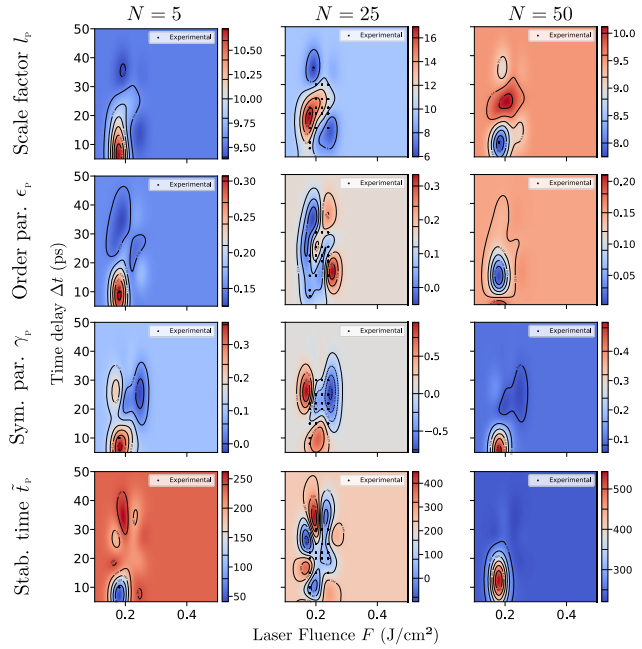

FIG. 4. Each plot shows, as a heat map, the ML model prediction of a single SH parameter (bottom to top: scale factor l_p; order parameter ϵ_p; symmetry breaking parameter γ_p; simulation stabilization time $\tilde{t}_p$) as a function of laser fluence, time delay, and number of pulses (respectively, x axis and y axis, and column). Experimental points are overlaid on each plot.

constant. Thus, varying l_p in the direction of ∇l_p allows adjusting the characteristic size of the particular stable mode defined by the other SH parameters. This opens the door to pattern optimization for specific applications.

Interestingly, (γ_p) determines whether holes or bumps are observed; $F = 0.2$ J/cm^2 separates a region of high and low γ_p, roughly independently of N; the sign of γ_p appears to be determined by F and Δt only. Furthermore, for large bifurcation parameter (ϵ_p), many modes are nonattenuated and patterns are less ordered. Correspondingly, large ϵ_p patches are observed at high F or low Δt (highest energy coupling). For $N = 25$, superimposing the $\gamma_p = 0$ isosurface on the ϵ_p prediction, it can be seen that it is roughly perpendicular to isosurfaces of ϵ_p. These abrupt transition regimes of ϵ_p are consistent with experimental observations where two patterns of different order are superimposed on the same SEM image. ($\tilde{t}_p$) for constant $l_p, \epsilon_p, \gamma_p$, symmetry increases with $\tilde{t}_p$, as symmetrical patterns require large $\tilde{t}_p$ to stabilize from a uniformly random state. As can be seen in the bottom row of Fig. 4, $\tilde{t}_p$ tends to increase with N, consistently with the physical view that a large N increases the time the dissipative system is in a far from equilibrium state. This increase is not uniform across F, Δt pairs, and the area of laser parameter space of relatively large $\tilde{t}_p$ decreases with N.

We show that ultrafast laser-irradiated surface nanoscale patterns can be numerically modeled by a scale-invariant generalized Swift-Hohenberg equation. A machine learning model is trained to learn the connection between the stochastic SH equation and laser parameters, independently of initial conditions, using a deep convolutional network to extract features and by incorporating physical information. Our original strategy can be applied generically to accurately predict the shape and scale of physical patterns resulting from diverse self-organization processes. Importantly, this applicability extends even to cases where the underlying physical model is approximate and the availability of experimental data is limited, including non-time series data. The ML model is able to identify regions of laser parameters that are relevant for applications and can even be used to predict novel patterns, since the convolutional neural network features are not learned from observed patterns. Regions where pattern superpositions are observed could be modeled more accurately via a mixing of SH processes, as a manifestation of superposed states of self-organization, providing new routes toward nanoscale surface manipulation by light.

This work has been funded by a public grant from the French National Research Agency (ANR) under the "France 2030" investment plan, which has the reference EUR MANUTECH SLEIGHT-ANR-17-EURE-0026.

Appendix A: Experimental setup.—In the proposed experiment, Mach-Zehnder interferometry was used to combine the effect of polarization mismatch with an adjustable interpulse delay Δt, enabling fine control of surface topography at the tens of nanometer scale [10]. By breaking the surface isotropy imposed by a single polarization state, a wide range of self-organization regimes was achieved on a nickel monocrystal oriented in the (001) direction. Specifically, using a cross-polarization strategy, setting a depolarization angle of $\alpha = 90°$ and a range of time delays between 8 and 25 ps were set, as shown in Fig. 1(a). The pulse duration was fixed at 150 fs, and the laser dose was finely controlled by the number N of double-pulse sequences. Prior to laser irradiation, the Nickel surface was mechanically polished with a Ra < 5 nm to ensure that the surface dynamics followed a hydrodynamics-governed process, smoothing the inhomogeneous electromagnetic response.

Appendix B: Image similarity.—It is important to note, regarding the ML strategy, that the problem is approached within the image of a feature mapping F_m, where the concept of similarity differs from visual similarity. In this feature space, an image is equivalent to any of its images in the orbit of the group of symmetries of F_m, such as translations, but also a variety of other symmetries that are learned from data automatically. Intuitively, similarity in feature space corresponds to similarity of patterns, which can be described in terms of, e.g., "bumpiness," "roundness," etc.

*jean.philippe.colombier@univ-st-etienne.fr

[1] T.-H. Her, R. J. Finlay, C. Wu, S. Deliwala, and E. Mazur, Microstructuring of silicon with femtosecond laser pulses, Appl. Phys. Lett. **73**, 1673 (1998).

[2] Y. Shimotsuma, P. G. Kazansky, J. Qiu, and K. Hirao, Self-Organized Nanogratings in Glass Irradiated by Ultrashort Light Pulses, Phys. Rev. Lett. **91**, 247405 (2003).

[3] S. Ilday, G. Makey, G. B. Akguc, Ö. Yavuz, O. Tokel, I. Pavlov, O. Gülseren, and F. Ö. Ilday, Rich complex behaviour of self-assembled nanoparticles far from equilibrium, Nat. Commun. **8**, 14942 (2017).

[4] J. E. Sipe, J. F. Young, J. S. Preston, and H. M. van Driel, Laser-induced periodic surface structure. I. Theory, Phys. Rev. B **27**, 1141 (1983).

[5] F. Keilmann, Laser-Driven Corrugation Instability of Liquid Metal Surfaces, Phys. Rev. Lett. **51**, 2097 (1983).

[6] J. F. Young, J. E. Sipe, and H. M. van Driel, Laser-induced periodic surface structure. III. Fluence regimes, the role of feedback, and details of the induced topography in germanium, Phys. Rev. B **30**, 2001 (1984).

[7] G. D. Tsibidis, E. Skoulas, A. Papadopoulos, and E. Stratakis, Convection roll-driven generation of supra-wavelength periodic surface structures on dielectrics upon irradiation with femtosecond pulsed lasers, Phys. Rev. B **94**, 081305(R) (2016).

[8] A. Rudenko, A. Abou-Saleh, F. Pigeon, C. Mauclair, F. Garrelie, R. Stoian, and J.-P. Colombier, High-frequency periodic patterns driven by non-radiative fields coupled with Marangoni convection instabilities on laser-excited metal surfaces, Acta Mater. **194**, 93 (2020).

[9] I. Prigogine and P. Van Rysselberghe, Introduction to thermodynamics of irreversible processes, J. Electrochem. Soc. **110**, 97C (1963).

[10] A. Nakhoul, C. Maurice, M. Agoyan, A. Rudenko, F. Garrelie, F. Pigeon, and J.-P. Colombier, Self-organization regimes induced by ultrafast laser on surfaces in the tens of nanometer scales, Nanomater. Nanotechnol. **11**, 1020 (2021).

[11] A. Nakhoul, A. Rudenko, C. Maurice, S. Reynaud, F. Garrelie, F. Pigeon, and J.-P. Colombier, Boosted spontaneous formation of high-aspect ratio nanopeaks on ultrafast laser-irradiated Ni surface, Adv. Sci. **9**, 2200761 (2022).

[12] E. Stratakis, J. Bonse, J. Heitz, J. Siegel, G. Tsibidis, E. Skoulas, A. Papadopoulos, A. Mimidis, A.-C. Joel, P. Comanns *et al.*, Laser engineering of biomimetic surfaces, Mater. Sci. Eng. R **141**, 100562 (2020).

[13] A. C. Overvig, S. C. Malek, and N. Yu, Multifunctional Nonlocal Metasurfaces, Phys. Rev. Lett. **125**, 017402 (2020).

[14] A. Rudenko, C. Mauclair, F. Garrelie, R. Stoian, and J.-P. Colombier, Self-organization of surfaces on the nanoscale by topography-mediated selection of quasi-cylindrical and plasmonic waves, Nanophotonics **8**, 459 (2019).

[15] O. Varlamova, F. Costache, J. Reif, and M. Bestehorn, Self-organized pattern formation upon femtosecond laser ablation by circularly polarized light, Appl. Surf. Sci. **252**, 4702 (2006).

[16] A. Abou Saleh, A. Rudenko, L. Douillard, F. Pigeon, F. Garrelie, and J.-P. Colombier, Nanoscale imaging of ultrafast light coupling to self-organized nanostructures, ACS Photonics **6**, 2287 (2019).

[17] R. Stoian and J.-P. Colombier, Advances in ultrafast laser structuring of materials at the nanoscale, Nanophotonics **9**, 4665 (2020).

[18] J. Bonse and S. Gräf, Maxwell meets Marangoni—a review of theories on laser-induced periodic surface structures, Laser Photonics Rev. **14**, 2000215 (2020).

[19] H. Qiao, J. Yang, J. Li, Q. Liu, J. Liu, and C. Guo, Formation of subwavelength periodic triangular arrays on tungsten through double-pulsed femtosecond laser irradiation, Materials **11**, 2380 (2018).

[20] F. Fraggelakis, G. Mincuzzi, J. Lopez, I. Manek-Hönninger, and R. Kling, Controlling 2D laser nano structuring over large area with double femtosecond pulses, Appl. Surf. Sci. **470**, 677 (2019).

[21] A. Abou Saleh, A. Rudenko, S. Reynaud, F. Pigeon, F. Garrelie, and J.-P. Colombier, Sub-100 nm 2D nanopatterning on a large scale by ultrafast laser energy regulation, Nanoscale **12**, 6609 (2020).

[22] M. Mastellone, A. Bellucci, M. Girolami, V. Serpente, R. Polini, S. Orlando, A. Santagata, E. Sani, F. Hitzel, and D. M. Trucchi, Deep-subwavelength 2D periodic surface nanostructures on diamond by double-pulse femtosecond laser irradiation, Nano Lett. **21**, 4477 (2021).

[23] R. M. Bradley and P. D. Shipman, Spontaneous Pattern Formation Induced by Ion Bombardment of Binary Compounds, Phys. Rev. Lett. **105**, 145501 (2010).

[24] J. Reif, O. Varlamova, S. Varlamov, and M. Bestehorn, The role of asymmetric excitation in self-organized nanostructure formation upon femtosecond laser ablation, in *AIP Conference Proceedings* (American Institute of Physics, Berlin/Heidelberg, 2012), Vol. 1464, pp. 428–441, 10.1007/s00339-011-6472-3.

[25] K. R. Elder, J. Vinals, and M. Grant, Ordering Dynamics in the Two-Dimensional Stochastic Swift-Hohenberg Equation, Phys. Rev. Lett. **68**, 3024 (1992).

[26] M. C. Cross and P. C. Hohenberg, Pattern formation outside of equilibrium, Rev. Mod. Phys. **65**, 851 (1993).

[27] W. Decker, W. Pesch, and A. Weber, Spiral Defect Chaos in Rayleigh-Bénard Convection, Phys. Rev. Lett. **73**, 648 (1994).

[28] B. Echebarria and H. Riecke, Defect Chaos of Oscillating Hexagons in Rotating Convection, Phys. Rev. Lett. **84**, 4838 (2000).

[29] N. Stoop, R. Lagrange, D. Terwagne, P. M. Reis, and J. Dunkel, Curvature-induced symmetry breaking determines elastic surface patterns, Nat. Mater. **14**, 337 (2015).

[30] J. Swift and P. C. Hohenberg, Hydrodynamic fluctuations at the convective instability, Phys. Rev. A **15**, 319 (1977).

[31] A. Tarantola, *Inverse Problem Theory and Methods for Model Parameter Estimation* (SIAM, PhilaPhiladelphia, 2005), 10.1137/1.9780898717921.

[32] A. Carrassi, M. Bocquet, L. Bertino, and G. Evensen, Data assimilation in the geosciences: An overview of methods, issues, and perspectives, Wiley Interdiscip. Rev. **9**, e535 (2018).

[33] M. C. Kennedy and A. O'Hagan, Bayesian calibration of computer models, J. R. Stat. Soc. Ser. B **63**, 425 (2001).
[34] F. A. Viana and A. K. Subramaniyan, A survey of Bayesian calibration and physics-informed neural networks in scientific modeling, Arch. Comput. Methods Eng. **28**, 3801 (2021).
[35] Y. Yin, V. Le Guen, J. Dona, E. de Bézenac, I. Ayed, N. Thome, and P. Gallinari, Augmenting physical models with deep networks for complex dynamics forecasting, J. Stat. Mech. (2021) 124012.
[36] T. Beucler, S. Rasp, M. Pritchard, and P. Gentine, Achieving conservation of energy in neural network emulators for climate modeling, arXiv:1906.06622.
[37] A. Filoche, J. Brajard, A. A. Charantonis, and D. Béréziat, Completing physics-based models by learning hidden dynamics through data assimilation, in *Proceedings of the Workshop AI4Earth, NeurIPS 2020* (2020), https://hal.sorbonne-universite.fr/hal-03004938.
[38] A. Farchi, P. Laloyaux, M. Bonavita, and M. Bocquet, Using machine learning to correct model error in data assimilation and forecast applications, Q. J. R. Meteorol. Soc. **147**, 3067 (2021).
[39] D. Nguyen, S. Ouala, L. Drumetz, and R. Fablet, Assimilation-based learning of chaotic dynamical systems from noisy and partial data, in *Proceedings of the ICASSP 2020-2020 IEEE International Conference on Acoustics, Speech and Signal Processing (ICASSP)* (IEEE, New York, 2020), pp. 3862–3866, 10.1109/ICASSP40776.2020.9054718.
[40] M. Déchelle, J. Donà, K. Plessis-Fraissard, P. Gallinari, and M. Levy, Bridging dynamical models and deep networks to solve forward and inverse problems, in *NeurIPS Workshop on Interpretable Inductive Biases and Physically Structured Learning* (2020), https://hal.science/hal-03739572.
[41] J. Bonse, J. Krüger, S. Höhm, and A. Rosenfeld, Femtosecond laser-induced periodic surface structures, J. Laser Appl. **24**, 042006 (2012).
[42] S. Wang, L. Jiang, W. Han, W. Liu, J. Hu, S. Wang, and Y. Lu, Controllable formation of laser-induced periodic surface structures on ZnO film by temporally shaped femtosecond laser scanning, Opt. Lett. **45**, 2411 (2020).
[43] E. Vitral, S. Mukherjee, P. H. Leo, J. Vinals, M. R. Paul, and Z.-F. Huang, Spiral defect chaos in Rayleigh-Bénard convection: Asymptotic and numerical studies of azimuthal flows induced by rotating spirals, Phys. Rev. Fluids **5**, 093501 (2020).
[44] E. Bodenschatz, W. Pesch, and G. Ahlers, Recent developments in Rayleigh-Bénard convection, Annu. Rev. Fluid Mech. **32**, 709 (2000).
[45] A. Thess and M. Bestehorn, Planform selection in Bénard-Marangoni convection: *l* hexagons versus *g* hexagons, Phys. Rev. E **52**, 6358 (1995).
[46] J. R. A. Pearson, On convection cells induced by surface tension, J. Fluid Mech. **4**, 489 (1958).
[47] R. V. Morgan, W. H. Cabot, J. A. Greenough, and J. W. Jacobs, Rarefaction-driven Rayleigh–Taylor instability. Part 2. Experiments and simulations in the nonlinear regime, J. Fluid Mech. **838**, 320 (2018).
[48] M. K. Smith and S. H. Davis, Instabilities of dynamic thermocapillary liquid layers. Part 1. Convective instabilities, J. Fluid Mech. **132**, 119 (1983).
[49] M. K. Smith, Instability mechanisms in dynamic thermocapillary liquid layers, Phys. Fluids **29**, 3182 (1986).
[50] G. D. Tsibidis, C. Fotakis, and E. Stratakis, From ripples to spikes: A hydrodynamical mechanism to interpret femtosecond laser-induced self-assembled structures, Phys. Rev. B **92**, 041405(R) (2015).
[51] F. H. Busse, Remarks on the critical value $P_c = 0.25$ of the Prandtl number for internally heated convection found by Tveitereid and Palm, Eur. J. Mech. B **47**, 32 (2014).
[52] T. Boeck and A. Thess, Bénard–Marangoni convection at low Prandtl number, J. Fluid Mech. **399**, 251 (1999).
[53] J. Bragard and M. G. Velarde, Bénard-Marangoni convection: Planforms and related theoretical predictions, J. Fluid Mech. **368**, 165 (1998).
[54] S. V. Starikov and V. V. Pisarev, Atomistic simulation of laser-pulse surface modification: Predictions of models with various length and time scales, J. Appl. Phys. **117**, 135901 (2015).
[55] See Supplemental Material at http://link.aps.org/supplemental/10.1103/PhysRevLett.130.226201, where electron microscopy images obtained through ultrafast irradiation, serving as a database for ML predictions, are provided. The SH nonlinear dynamics model of convection and the machine learning approach utilized in this study are also comprehensively explained. Additionally, the physical timescale of convective instability is originally derived from the ML outcomes.
[56] G. Strang, On the construction and comparison of difference schemes, SIAM J. Num. Anal. **5**, 506 (1968).
[57] R. J. LeVeque, *Finite Difference Methods for Ordinary and Partial Differential Equations: Steady-State and Time-Dependent Problems* (SIAM, Philadelphia, 2007), 10.1137/1.9780898717839.bm.
[58] H. Yoshida, Construction of higher order symplectic integrators, Phys. Lett. A **150**, 262 (1990).
[59] J. W. Cooley and J. W. Tukey, An algorithm for the machine calculation of complex fourier series, Math. Comput. **19**, 297 (1965).
[60] J. C. Butcher, *Numerical Methods for Ordinary Differential Equations* (John Wiley & Sons, New York, 2016), 10.1002/9781119121534.
[61] S. Greydanus, M. Dzamba, and J. Yosinski, Hamiltonian neural networks, Adv. Neural Inf. Process. Syst. **32** (2019), https://proceedings.neurips.cc/paper/2019/hash/26cd8ecadce0d4efd6cc8a8725cbd1f8-Abstract.html.
[62] V. Vapnik, *The Nature of Statistical Learning Theory* (Springer Science & Business Media, New York, 1999), 10.1007/978-1-4757-2440-0.
[63] Y. LeCun, L. Bottou, Y. Bengio, and P. Haffner, Gradient-based learning applied to document recognition, Proc. IEEE **86**, 2278 (1998).
[64] J. Deng, W. Dong, R. Socher, L.-J. Li, K. Li, and L. Fei-Fei, Imagenet: A large-scale hierarchical image database, in *Proceedings of the IEEE Conference on Computer Vision and Pattern Recognition, 2009* (IEEE, New York, 2009), pp. 248–255, 10.1109/cvpr.2009.5206848.

[65] M. Graziani, T. Lompech, H. Müller, A. Depeursinge, and V. Andrearczyk, On the scale invariance in state of the art CNNs trained on imagenet, Mach. Learn. Knowl. Extr. **3**, 374 (2021).

[66] C. M. Bishop and N. M. Nasrabadi, *Pattern Recognition and Machine Learning* (Springer, New York, 2006), Vol. 4.

[67] H. Drucker, C. J. Burges, L. Kaufman, A. Smola, and V. Vapnik, Support vector regression machines, Adv. Neural Inf. Process. Syst. **9**, 155 (1996), https://proceedings.neurips.cc/paper_files/paper/1996/hash/d38901788c533e8286cb6400b40b386d-Abstract.html.